

# Holographic Nearfield Measurement of Loudspeaker Directivity

Wolfgang Klippel, Christian Bellmann, Klippel GmbH, Dresden 01309, Germany

The acoustical output of loudspeaker systems is usually measured in the far field under anechoic conditions requiring a large measurement distance and special treatment of the room (absorbing room boundaries, air condition). Also, the measurements of directivity characteristics at sufficient angular resolution are very time consuming. The measurement in the near field of the sound source provides significant benefits (dominant direct sound, higher SNR, less climate impact) but requires a scanning process and a holographic processing of the measured data. This paper describes the theoretical basis of this new measurement technique and practical consequences for the loudspeaker diagnostics.

## 1. Introduction

Traditionally, the acoustical output and directivity of the loudspeaker are measured in far field ( $r > r_{far}(f)$ ) where the sound pressure is in-phase with the particle velocity and the amplitude decreases inversely with the distance  $r$  from the acoustical center. Therefore, it is convenient to describe the sound pressure  $p(\mathbf{r})$  in the far field in spherical coordinates

$$\mathbf{r} = \begin{pmatrix} x \\ y \\ z \end{pmatrix} = \mathbf{r}_{ref} + r \begin{pmatrix} \cos(\phi)\sin(\theta) \\ \sin(\phi)\sin(\theta) \\ \cos(\theta) \end{pmatrix} \quad (1)$$

where the origin is placed at the reference point  $\mathbf{r}_{ref}$  defined at a convenient place on the surface of radiator, grill or enclosure, close to the supposed acoustical center. The reference axis  $\mathbf{n}_{ref}$  is usually orthogonal to the radiators surface and the orientation vector  $\mathbf{o}_{ref}$  usually points in vertical direction.

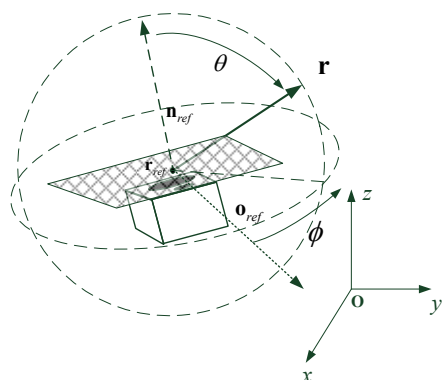


Figure 1 Standard coordinate system used to assess the far field properties of a loudspeaker system

### 1.1. Far-field condition

The minimum distance  $r_{far}(f)$  where the far field is reached varies with frequency  $f$  and depends on the particular geometry of the loudspeaker. Comparing the maximum geometrical dimension  $d$  of the loudspeaker with the wavelength  $\lambda=c_0/f$ , the minimum distance  $r_{far}$  has to fulfill all of the following conditions:

1.  $r_{far} > d$
2.  $r_{far} > \lambda$  (critical at low frequencies)
3.  $r_{far}/d > d/\lambda$  (critical at high frequencies)

For line arrays, sound bars and other large loudspeakers measured over the audio band, the minimum distance exceeds typically 5 m. There is significant effort required to ensure anechoic and constant propagation conditions in the air in the far field and sufficient suppression of the ambient noise. An anechoic room is the best solution to cope with wind, climate changes and noise but is a cost intensive and long term investment that cannot be moved to other locations. Measurements at larger distances also reveal the imperfections of the anechoic room such as an error ( $> 1\text{dB}$ ) in the measured amplitude response at low frequencies ( $< 100\text{Hz}$ ) due to the limited depth absorption material lining of the room boundaries. The measurement of the amplitude response in the far field at high frequencies can be accomplished with high accuracy because the positioning error has a minor influence and reflections can be removed by windowing the impulse response. However, the temperature of the air in the propagation path has a significant influence on the speed of sound  $c_0$  and the measured phase response at high frequencies. For example, an increase of the air temperature by 2 Kelvin over a distance  $r=5$  m will already generate a phase error of  $90^\circ$  at 5 kHz. Climate conditioning can control the mean temperature in the room but it is very difficult to ensure a homogenous temperature field. Thus, far field measurements are less suited for providing the accurate phase information at higher frequencies that is required

for optimal installations of line arrays and active systems using beam steering.

## 1.2. Angular Resolution

The main advantage of the far-field measurement is that all relevant information of the 3D sound field is mapped to the sound distribution on a 2D surface with a constant distance  $r$  (radius of the sphere) from the reference point that only depends on two angles, latitude  $\theta$  and azimuth  $\phi$ . This directivity characteristic can be measured traditionally by turning the loudspeaker around the reference point  $\mathbf{r}_{ref}$  or by using a microphone array placed on a sphere with the radius  $r$ . The angular resolution corresponds to the angular increments of the turntable or the angular difference between adjacent microphone positions. Sampling the complete sphere at  $1^\circ$  angular resolution would require 64.800 single measurement points. In practice, the total number of measurement point has to be significantly reduced to keep the total measurement time acceptable. A coarser angular resolution ( $\geq 2^\circ$ ) may be sufficient for small loudspeaker operated at low frequencies where the source has low directivity, then various kinds of interpolation techniques can be applied to approximate the polar pattern. However, the same angular resolution may produce spatial aliasing on other loudspeakers at higher frequencies where nulls and lobes are not detected, and significant errors are introduced in the sound power response and other directional characteristics. This problem cannot be detected by post-processing if the directivity pattern of the loudspeaker is unknown.

In practice, the traditional far field measurement technique requires a compromise between measurement effort and accuracy, which depends on the experience and intuition of the user. There are major uncertainties and no objective way to assess the reliability of the generated data. This is an unsatisfying situation which can be solved by physical modeling of the sound radiation and by checking the consistency of the measured data.

## 2. Spherical Wave Expansion

The sound propagation between the loudspeaker surface and other external boundaries (e.g. room walls) can be described by the Helmholtz equation. Using spherical coordinates

$$\mathbf{r}_E = \begin{pmatrix} x \\ y \\ z \end{pmatrix} = \mathbf{r}_{EP}(f) + r_E \begin{pmatrix} \cos(\phi_E(f)) \sin(\theta_E(f)) \\ \sin(\phi_E(f)) \sin(\theta_E(f)) \\ \cos(\theta_E(f)) \end{pmatrix} \quad (2)$$

the solution of the Helmholtz equation can be separated into radial and angular functions which form a complete and orthogonal set of base solution corresponding to spherical waves having their center in the expansion point  $\mathbf{r}_{EP}(f)$ . Contrary to the standard coordinate system in Figure 1, the expansion point  $\mathbf{r}_{EP}(f)$  might be not directly accessible (e.g. inside the enclosure), and the position of this point and the orientation of angles  $\theta_E(f)$  and  $\phi_E(f)$  might change with frequency.

Introducing a transfer function  $H(f, \mathbf{r}_E) = P(f, \mathbf{r}_E)/U(f)$  between the input signal  $u$  and the sound pressure  $p(t)$  in the frequency domain, the transfer function can be expanded into a series of base solutions weighted by coefficients  $\mathbf{c}(f)$ :

$$H(f, \mathbf{r}_E) = \sum_{n=0}^{N(f)} \sum_{m=-n}^n C_{mn}(f) \cdot h_n^{(2)}(kr_E) Y_n^m(\theta_E, \phi_E) = \mathbf{c}(f) \mathbf{b}(f, \mathbf{r}_E) \quad (3)$$

The base solution  $\mathbf{b}(f, \mathbf{r}_E)$  uses the spherical harmonics

$$Y_n^m(\theta_E, \phi_E) = \sqrt{\frac{(2n+1)(n-m)!}{4\pi(n+m)!}} P_n^m(\cos \theta_E) e^{jm\phi_E} \quad (4)$$

to describe the angular dependency on the latitude angle  $\theta_E$  by using the Legendre function  $P_n^m$  and the dependency on  $\phi_E$  by a complex exponential function.

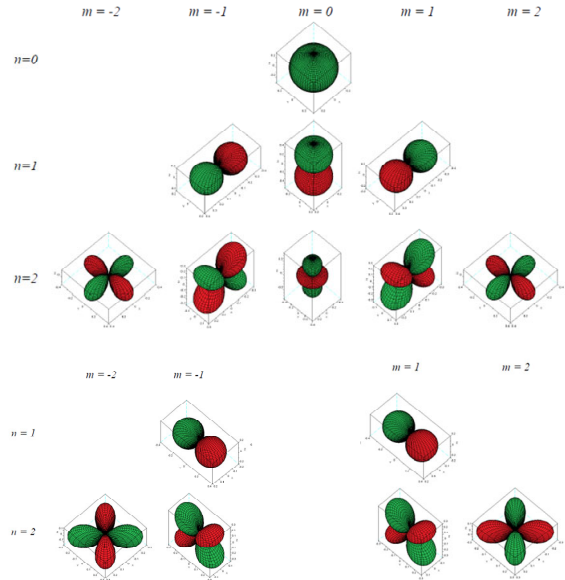


Figure 2 Real part (above) and imaginary part (below) of the spherical harmonics  $Y_n^m(\theta_E, \phi_E)$  versus order  $n$  and suborder  $m$

Figure 2 shows the real and imaginary part of the spherical harmonics versus order  $n=0,1,2$  and suborder  $m=-n, \dots, n$ . The zero order function describes the omnidirectional characteristic of a monopole while the first

order harmonics  $n=1$  describes the orientation of dipole in any direction.

The radial dependency on the distance  $r_E$  between point  $\mathbf{r}_E$  and the expansion point  $\mathbf{r}_{EP}(f)$  is separated in the Hankel function of the second kind

$$\begin{aligned} h_n^{(2)}(kr_E) &= j_n(kr_E) - iy_n(kr_E) \\ &\approx i \frac{(2n-1)!!}{(kr_E)^{n+1}} \quad kr_E < 1 \\ &\approx i^{n+1} \frac{e^{-ikr_E}}{kr_E} \quad kr_E > 1 \end{aligned} \quad (5)$$

using the wavenumber  $k=2\pi f/c_0$ , the  $n^{\text{th}}$ -order Bessel function  $j_n$  and  $n^{\text{th}}$ -order Neumann function  $y_n$ , which are plotted versus  $kr_E$  in Figure 3.

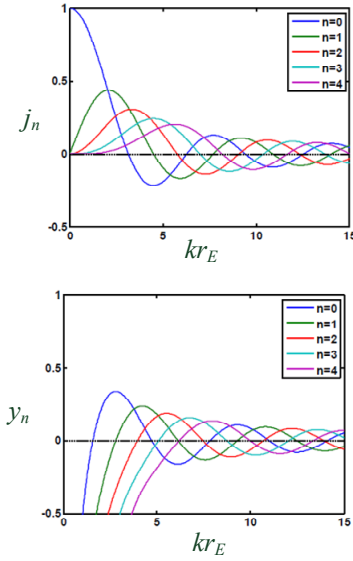


Figure 3 Bessel function  $j_n$  (above) and Neumann function  $y_n$  (below) of order  $n$  versus  $kr_E$

The Hankel function of the 2<sup>nd</sup> kind describes the phase and amplitude of spherical waves diverging from the expansion point to infinity. For large arguments of  $kr_E$ , the amplitude decreases by  $1/r_E$  and the phase varies with  $kr_E$ . For small arguments, the Neumann function  $y_n$  becomes dominant in the Hankel function, approaching negative infinity at the expansion point.

The complex coefficients  $C_{mn}(f)$  are the free parameters of the model that have to be estimated for the particular device under test.

J. Angus, et. al. [9] applied the spherical wave expansion to loudspeaker far field data that is measured spherically, centered at the expansion point  $\mathbf{r}_{EP}$ , and coefficients  $C_{mn}$  are estimated by integrating the measured data weighted by the spherical harmonics on the sphere. Alternatively, Lu, et. al. [13] suggested to estimate the coefficients  $C_{mn}$  by minimizing the squared error between modeled and measured far field data collected on any arbitrarily shaped closed surface around the loudspeaker [11].

If the coefficients  $C_{mn}(f)$  are determined for the particular loudspeaker, the transfer function  $H(f, \mathbf{r}_E)$  can be calculated according to Eq. (3) for any point  $\mathbf{r}_E$  outside the scanning surface.

### 3. Near-Field Measurement

The measurement in the near field of the loudspeaker seems interesting because the amplitude of direct sound is significantly increased compared to the room reflections and any other ambient noise. Furthermore, the influence of air properties (humidity, temperature and wind) on the measured phase response is negligible. However, the near field shows a much higher complexity, and holographic post processing is required to generate the far field data.

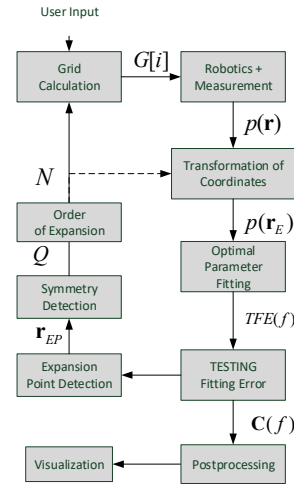


Figure 4 Overview of near field measurement and holographic post-processing

Figure 4 gives an overview of the near-field measurement that is organized as an iterative procedure. By setting up the scanner system, the user provides valuable information on the maximum size of the loudspeaker, the location of the reference point  $\mathbf{r}_{ref}$  and the reference axis  $\mathbf{n}_{ref}$ , which are useful initial values for the location of the expansion point  $\mathbf{r}_{EP}$  and the orientation of the angles  $\theta_E$  and  $\phi_E$ .

#### 3.1. Scanning Process

The sound pressure distribution in the near field of the loudspeaker has to be sampled with small positioning error ( $< 3$  mm) to ensure sufficient accuracy of the holographic reconstruction of the 3D sound field at high frequencies. Keeping the microphone at a fixed position requires powerful robotics to turn large and heavy loudspeaker over two orthogonal axes. A single microphone can be moved at a much higher speed using light and more cost effective actuators. It is also

beneficial for scanning on multiple layers to separate the sound components reflected at room boundaries and at the gear close to the non-moving loudspeaker (sound field separation technique [21], [22]).

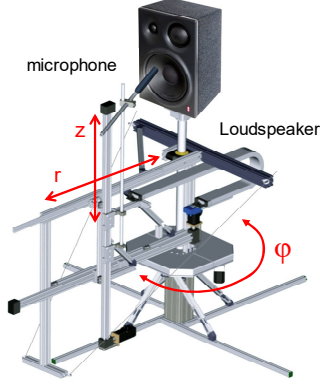


Figure 5 Robotics used for loudspeaker near field scanning in cylindrical coordinates  $(r, z, \varphi)$

Figure 5 shows a first realization of a 3D near field scanner in cylindrical coordinates. The loudspeaker is placed in a fixed position on a post while heavy loads ( $> 100\text{kg}$ ) are supported by a crane. This design has almost no gears inside the scanning grid and the reflection on gears outside the scanning grid can be reduced by field separation [21], [22] at low frequencies and windowing of the impulse response at high frequencies. Multiple microphones would reduce the scanning time but increase the microphone requirements and make the calibration of the microphone position more critical. As a single sensor, a low cost microphone can be used because the distortion in the phase and amplitude response of the microphone will not affect the holographic identification of the sound field, and the measured frequency response can be corrected by the same inverse microphone transfer function.

A second noise microphone may be placed at a fixed position and to repeat the measurement at the particular scanning point if the measured sound pressure at the first microphone is corrupted by ambient noise.

### 3.2. Measurement Grid

The generation of the measurement grid in the near field is much more critical than in the far field because the close distance to the acoustical center may cause spatial aliasing at higher frequencies while using a minimum number of points. Thus, the measurement grid

$$\begin{aligned} G[1] &= L_1 = \{\mathbf{r}_1, \mathbf{r}_1, \dots, \mathbf{r}_E, \dots\} \\ G[2] &= \{L_1 + L_2\} \\ G[3] &= \{L_1 + L_2 + L_3\} \\ &\vdots \end{aligned} \quad (6)$$

is developed iteratively by using the user input for the first grid  $G[1]$  and using the information from holographic processing of the measurement data for optimal placing of additional measurement points. This creates a non-uniform sampling grid.

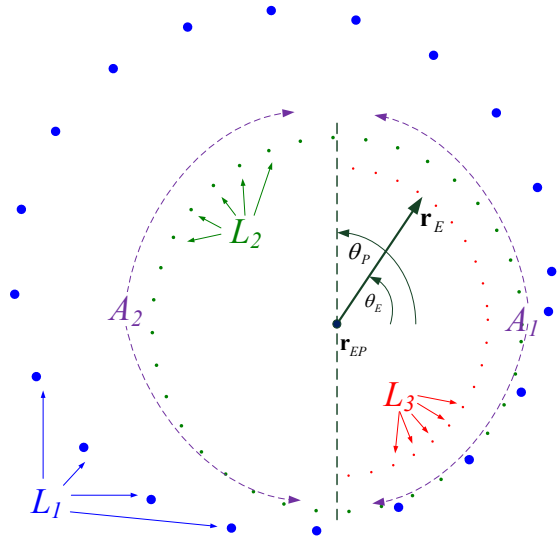


Figure 6 Iterative development of the scanning grid  $G[i]$

For example, Figure 6 shows a sparse sampling in subset  $L_1$  that is the basis for identifying an optimum position of the expansion point  $\mathbf{r}_{EP}(f)$ , which is close to the acoustical center at high frequencies, and to identify the symmetry properties of the loudspeaker. This information is used to generate the second subset  $L_2$  of additional measurement points located at a shorter distance from the expansion point and spaced with sufficient angular resolution to satisfy the spatial sampling on the rear side of the loudspeaker. The third subset  $L_3$  of points is placed on the front side of the loudspeaker to identify the coverage angle of the main lobe at higher accuracy.

### 3.3. Coordinate Transformation

The first step in the holographic data processing is a transformation of the original coordinates  $\mathbf{r}$  of all measurement points into coordinates

$$\mathbf{r}_E(f) = \mathbf{Q}(f)\mathbf{r} + \mathbf{r}_{EP}(f) - \mathbf{r}_{ref} \quad (7)$$

which are optimal for the following parameter fitting. Not only the expansion point  $\mathbf{r}_{EP}(f)$  but also the rotation matrix  $\mathbf{Q}(f)$  might vary with frequency.

### 3.4. Global Parameter Fitting

The global parameter fitting determines the optimum values  $C_{mn}$  in the parameter vector

$$\mathbf{c}(f) = \arg \min_{\mathbf{c}(f)} \left( \sum_{\forall \mathbf{r}_E \in G} |e(f, \mathbf{r}_E)|^2 \right) \quad (8)$$

by minimizing the deviation

$$e(f, \mathbf{r}_E) = H_m(f, \mathbf{r}_E) - H(f, \mathbf{r}_E) \quad (9)$$

between measured and modelled transfer function,  $H_m(f, \mathbf{r}_E)$  and  $H(f, \mathbf{r}_E)$ , respectively.

The error for all measurement points  $\mathbf{r}_E$  of the measurement grid can be rewritten in matrix form:

$$\begin{aligned} \mathbf{e}(f) &= \mathbf{H}_m(f) - \mathbf{c}(f)\mathbf{B}(f) \\ &= \begin{bmatrix} H_m(f, \mathbf{r}_1) \\ \vdots \\ H_m(f, \mathbf{r}_E) \\ \vdots \\ H_m(f, \mathbf{r}_M) \end{bmatrix} - \mathbf{c}(f) \begin{bmatrix} \mathbf{b}(f, \mathbf{r}_1) \\ \vdots \\ \mathbf{b}(f, \mathbf{r}_E) \\ \vdots \\ \mathbf{b}(f, \mathbf{r}_M) \end{bmatrix} \end{aligned} \quad (10)$$

The optimal parameter vector  $\mathbf{c}(f)$

$$\mathbf{c}(f) = \mathbf{H}(f)\mathbf{B}(f)(\mathbf{B}(f)\mathbf{B}(f)^H)^{-1} \quad (11)$$

can be calculated by using the pseudo-inverse of  $\mathbf{B}(f)$  from a numerically robust technique (e.g. QR decomposition).

### 3.5. Verification

The redundancy in the measured data allows assessment of the accuracy of the holographic modeling of the sound field. The total fitting error ( $TFE$ ) defined as

$$TFE(f) = 10 \log \left( \frac{\sum_{\mathbf{r}_E \in G} |e(f, \mathbf{r}_E)|^2}{\sum_{\mathbf{r}_E \in G} |H(f, \mathbf{r}_E)|^2} \right) \quad (12)$$

is comprised of the truncation of the power series at maximum order  $N$ , positioning error during scanning, reflections on acoustical boundaries and ambient and measurement noise. If the  $TFE(f)$  is smaller than -20 dB, the model describes the measured data with sufficient accuracy.

The multi-layer error

$$MLE(f) = 10 \log \left( \frac{\sum_{\mathbf{r}_E \in G_1} |e(f, \mathbf{r}_E) - e'(f, \mathbf{r}_E)|^2}{\sum_{\mathbf{r}_E \in G_1} |H(f, \mathbf{r}_E)|^2 + |H(f, \mathbf{r}'_E)|^2} \right) \quad (13)$$

checks the agreement between error  $e(f, \mathbf{r}_E)$  at the first point  $\mathbf{r}_E$  on the outer layer  $L_1$  in Figure 6 and the error  $e(f, \mathbf{r}'_E)$  at the closest point  $\mathbf{r}'_E$  on the inner layers  $\{L_2, L_3\}$  which can be found at the maximum of the scalar product:

$$\mathbf{r}'_E = \arg \max_{\forall \mathbf{r}'_E} \frac{\langle \mathbf{r}_E, \mathbf{r}'_E \rangle}{\|\mathbf{r}_E\| \|\mathbf{r}'_E\|} \quad \forall \mathbf{r}'_E \in L_1 \quad (14)$$

To consider the different distances of the two scanning points from the expansion point the error  $e(f, \mathbf{r}'_E)$  is extrapolated to position  $\mathbf{r}_E$  by equation:

$$e'(f, \mathbf{r}_E) = \frac{H(f, \mathbf{r}_E)}{H(f, \mathbf{r}'_E)} e(f, \mathbf{r}'_E) \quad (15)$$

If the errors  $TFE$  and  $MLE$  are in the same order of magnitude, the measurement is corrupted by noise, room reflections or positioning errors.

### 3.1. Order of Expansion

An increase of the maximum order  $N$  would improve the angular resolution if the total fitting error  $TFE(f)$  is much larger than the multi-layer error  $MLE(f)$ . This is illustrated in Figure 7, where the  $TFE(f)$  shown in the upper diagram decreases with rising order  $N$ .

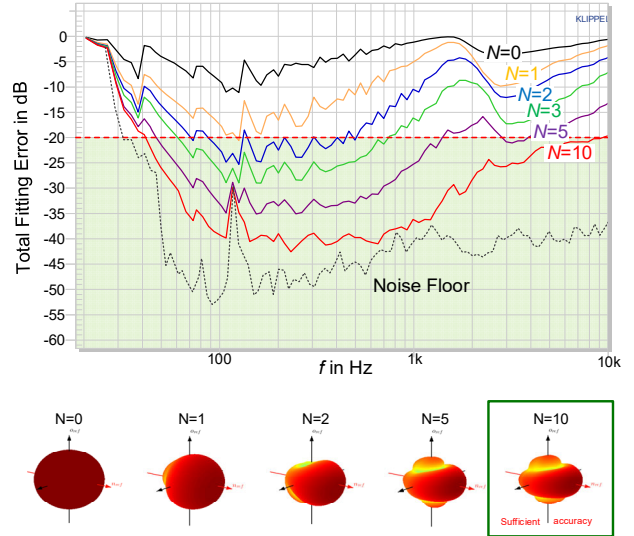


Figure 7 Total fitting error  $TFE(f)$  in dB versus frequency  $f$  for 5 wave expansion with maximum order  $N$ .

The wave expansion truncated after order  $N=10$  is capable of modeling the 3D output above 30 Hz with sufficient accuracy ( $TFE < -20$  dB). At very low frequencies ( $f < 30$  Hz) the higher order terms of the expansion can only slightly reduce the  $TFE$  that is mainly caused by the poor  $SNR$  below the cut-off frequency of the particular device. The scanning at multiple points at

different distances but similar directions generates a valuable redundancy in the data and prevents interpretation of measurement noise as directional information.

#### 4. Minimum Test Time

The wave expansion in Eq. (3) of maximum order  $N$  contains  $J=(N+1)^2$  coefficients in vector  $\mathbf{c}(f)$ , and their fitting requires a larger number of measurements points (usually  $M > 1.5J$ ) to avoid spatial aliasing and to verify the accuracy of the results. Although the sound pressure measurement in the near field of the loudspeaker provides a good  $SNR$  without additional averaging, the total measurement cycle, including positioning, will take more than 3 s. Thus, the scanning process dominates the duration of the holographic measurement. However, there are many ways to optimize the performance and speed of the measurements.

##### 4.1. Expansion Point

The optimum position of the expansion point  $\mathbf{r}_{EP}(f)$ , especially at high frequencies  $f$ , significantly reduces the total fitting error and the order  $N$  required to bring the  $TFE$  down to -20 dB. User information about the position of the tweeter is needed, or signal processing can automatically localize the acoustical center at the particular frequency  $f$  based on the measured data and identified wave expansion.

The knowledge about the optimal expansion point  $\mathbf{r}_{EP}(f)$  also has consequences for the grid generation. For example, the grid  $G[1]$  shown in Figure 6 was created based on user input information, and the holographic processing data leads to correcting the expansion point and a corresponding shift of the center of the scanning grids  $G[i]$  with  $i \geq 2$ .

##### 4.2. Partial Fitting

At high frequencies, horn loaded compression drivers and many other loudspeakers are directive and generate a much smaller sound on the rear side. To assess the coverage angle on those devices, a higher angular resolution is required on the front side with  $\theta_E < 90^\circ$  than on the rear side with  $\theta_E > 90^\circ$ . To solve this problem, separate wave expansions

$$H_m(f, \mathbf{r}_E) = \mathbf{c}_i(f) \mathbf{b}(f, \mathbf{r}_E) \quad \forall \mathbf{r}_E \in A_i \quad (16)$$

with a particular order  $N_i$  to pairwise disjunctive angular sets  $A_i$  of the scanning grid  $G = \{A_1, A_2, A_i, \dots\}$  are applied. For example, Figure 6 shows a partition of the grid  $G$  into two segments on the sphere separated at angle  $\theta_p = 90^\circ$ :

$$\begin{aligned} A_1 &= \{\forall \mathbf{r}_E \in G \text{ with } 0 \leq \theta_E < \theta_p\} \\ A_2 &= \{\forall \mathbf{r}_E \in G \text{ with } \theta_p \leq \theta_E \leq \pi\} \end{aligned} \quad (17)$$

The number of sampling points is much higher in set  $A_1$  on the front side than in set  $A_2$  on the rear side. Thus, the estimation of the coefficients

$$\mathbf{c}_i(f) = \arg \min_{\mathbf{c}_i(f)} \left( \sum_{\forall \mathbf{r}_E \in A_i} |e(f, \mathbf{r}_E)|^2 \right) \quad (18)$$

with order  $N_1 > N_2$  gives the requested higher resolution on the front side and natural interpolation on the rear side. Optionally, post processing can be used to merge the two wave expansions to a single expansion with the order  $N_I$ .

#### 4.3. Exploiting Symmetry

Many loudspeakers have rotational or plane symmetries in the geometrical shape of the radiator or enclosure, yielding symmetries in the sound field. This property can be used to reduce the number of coefficients and the scanning effort [7]. The operator of the scanner can provide useful information about the loudspeaker geometry explicitly by user input or implicitly by following general instructions on how to place the loudspeaker on the scanner by using the reference point  $\mathbf{r}_{ref}$ , reference axis  $\mathbf{n}_{ref}$  and orientation vector  $\mathbf{o}_{ref}$ . After performing the first holographic processing based on the coarse grid  $G[1]$ , the symmetry information can be checked and the internal coordinate system can be corrected automatically. The confirmed symmetry can be used to generate finer grids  $G[2]$  and  $G[3]$  that should have an asymmetrical structure, where the measurement points are interlaced on both sides of the symmetry axis. Mirroring this distribution to the other side will double the angular resolution and smooth the error caused by a small residual asymmetry in the field.

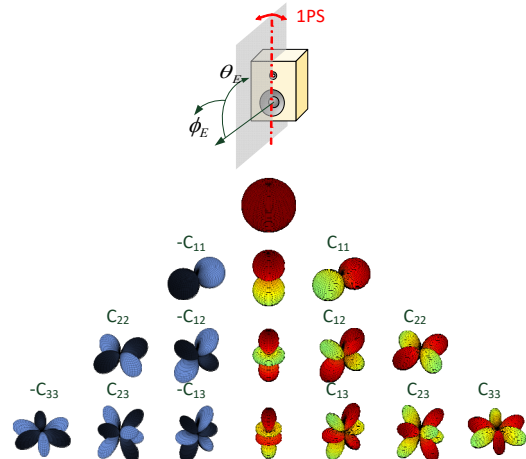


Figure 8 Relationship between the coefficients of the wave expansion for a single plane symmetry (1PS) at symmetry angle  $\phi_s=0$

#### 4.3.1. Single Plane Symmetry

The most common symmetry in loudspeakers using multiple transducers (woofer, midrange, tweeter) is single plan symmetry at angle  $\phi_E$ , which corresponds to the orientation  $\mathbf{o}_{ref}$  in vertical direction, as illustrated in Figure 8.

This symmetry generates the following relationship in the coefficients

$$C_{mn}(f) = C_{-mn}(f)R_m(f) \quad \text{with } m \geq 0 \quad (19)$$

with the complex symmetry parameter [17]

$$R_m(f) = (-1)^{m+1} (\sin(m\phi_s(f)) + i \cos(m\phi_s(f)))^2 \quad (20)$$

that generates a defined coupling between coefficients of the suborder  $\pm m$ . If the symmetry axis is aligned to the coordinate system ( $\phi_s=0$ ), only the coefficients on the left side ( $m \leq 0$ ) have to be estimated, and the coefficients on the right side can be calculated by

$$C_{mn}(f) = C_{-mn}(f)(-1)^m \quad \text{with } \begin{matrix} 0 \leq m \\ 0 \leq n \leq N \end{matrix} \quad (21)$$

if the following measure evaluating the single plane symmetry (1PS)

$$S_{1PS} = 1 - \frac{\sum_{n=1}^N \sum_{m=1}^n |(-1)^m (f) C_{-mn} - C_{mn}|^2}{\sum_{n=0}^N \sum_{m=-n}^n C_{mn}^2} \quad (22)$$

exceeds a predefined limit value (e.g.  $S_{1PS} > 0.95$ ).

This reduces the number of unknown parameters to

$$J = \frac{(N+1)(N+2)}{2} \quad (23)$$

and the scanning effort by 50 %.

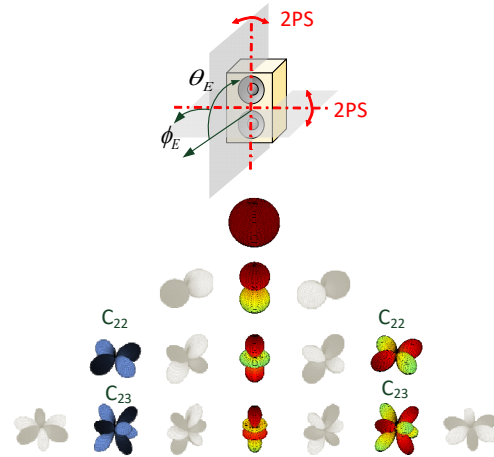


Figure 9 Relationship between the coefficients of the wave expansion for a dual plane symmetry (2PS) at symmetry angles  $\phi_s = 0, 90^\circ$

#### 4.4. Dual Plane Symmetry

Subwoofers or other loudspeakers using a single loudspeaker placed symmetrically in a rectangular enclosure may have a dual plane symmetry as illustrated in Figure 9.

In this case, half of the coefficients vanish completely and the most of the remaining coefficients are pairwise related by

$$C_{mn}(f) = C_{-mn}(f)R_m(f) \quad m = 2s, s = 1, 2, 3, \dots \quad (24)$$

with  $R_m(f)$  according Eq. (20). If the symmetry axes are aligned with the coordinate system ( $\phi_s = 0, 90^\circ$ ), the following coefficients can be calculated by the relationship:

$$C_{mn}(f) = C_{-mn}(f)(-1)^m \quad \begin{matrix} m = 2s \\ s = 1, 2, 3 \end{matrix} \quad (25)$$

If the measure of the dual plane symmetry

$$S_{2PS} = 1 - \frac{\sum_{n=2}^N \sum_{s=1}^{n/2} |(-1)^{2s} C_{2s,n} - C_{2s,n}|^2 + \sum_{n=1}^N \sum_{s=0}^{n/2} |C_{2s+1,n}|^2}{\sum_{n=0}^N \sum_{m=-n}^n C_{mn}^2} \quad (26)$$

exceeds a predefined limit, the total number of coefficients can be reduced to

$$J = \begin{cases} \left(\frac{N}{2} + 1\right)^2 & N = 0, 2, 4, \dots \\ \left(\frac{N}{2} + 1\right)^2 + \frac{1}{4} & N = 1, 3, 5, \dots \end{cases} \quad (27)$$

and the scanning effort by 70 %.

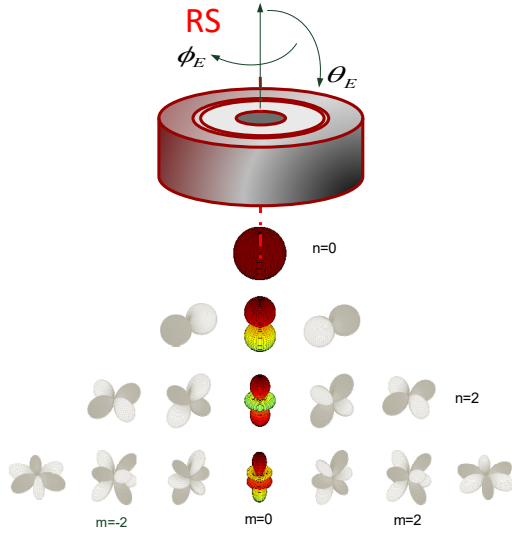


Figure 10 Nonzero coefficients of the wave expansion rotational symmetry (RS)

#### 4.5. Rotational Symmetry

A significant number of radiators and transducers used in loudspeakers have a round shape and generate a rotational symmetry in the generated sound field if the influence of diffraction on the enclosure is negligible. If the rotational axis agrees with  $\theta_E=0$ , the coefficients

$$C_{mn} = 0 \quad m \neq 0 \quad (28)$$

of all asymmetrical spherical harmonics vanish, as depicted in Figure 10. Only  $N+1$  coefficients have to be estimated if the measure of the rotational symmetry

$$S_{RS} = 1 - \frac{\sum_{n=1}^N \sum_{s=1}^n |C_{sn}|^2}{\sum_{n=0}^N \sum_{m=-n}^n C_{mn}^2} \quad (29)$$

exceeds a predefined limit value. This reduces the scanning effort by 97 %.

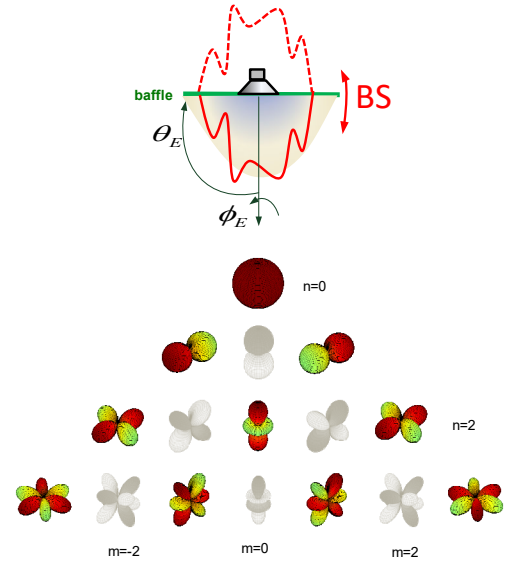


Figure 11 Non-zero coefficients of the wave expansion for a transducer mounted in an infinite baffle (BS)

#### 4.6. Baffle Symmetry

The radiated sound pressure is doubled by a mirrored sound source while operating transducers in a half space or in a baffle, as shown in Figure 10. If the normal vector of the baffle equals the coordinate at  $\theta_E=0$  half of the coefficients

$$C_{mn} = 0 \quad n - m \neq 2s \quad |s \in \mathbb{Z} \quad (30)$$

vanish. If the measure of the Baffle symmetry

$$S_{BS} = 1 - \frac{\sum_{n=1}^N \sum_{s=0}^{n/2} |C_{(2s)n}|^2}{\sum_{n=0}^N \sum_{m=-n}^n C_{mn}^2} \quad (31)$$

exceeds a predefined limit value, the coefficients in Eq. (30) are set to zero. This reduces the total number of coefficients to

$$J = \frac{(N+1)(N+2)}{2} \quad (32)$$

and the scanning effort by 50 %.

Table 1 Reduction of the total number of coefficients and scanning effort by exploiting symmetry of the sound field ( $N=30$ )

Symmetry	Number of Coefficients	Reduction of measurement samples
No Symmetry	961	0 %

Baffle Symmetry	496	48 %
Single plane symmetry	496	48 %
Dual plane symmetry	256	73 %
Rotational symmetry	31	97 %
Single plan symmetry + Baffle Symmetry	256	73 %
Dual plane symmetry + Baffle Symmetry	136	86 %
Rotational + Baffle	16	98 %

Table 1 gives an example of the reduction of the number of coefficients and the possible saving of the scanning effort for modeling a complex sound field of loudspeaker by a wave expansion with maximum order  $N=30$  while exploiting various kinds and combinations of symmetries.

## 5. Post-Processing

The coefficients  $C_{nm}(\mathbf{r}_{EP}(f), f)$  of the wave expansion identified for the particular loudspeaker are a convenient basis for further post-processing, presenting the results in a standard format and simplifying the interpretation.

### 5.1. Standard Output Format

The near field scanning and holographic processing use an internal, frequency depending coordinate system to combine higher accuracy with a minimum scanning effort. The coefficients  $C_{nm}(f)$  depending on a useful choice of the expansion point  $\mathbf{r}_{EP}(f)$ , and the rotation matrix  $\mathbf{Q}(f)$  also gives some benefits for the development of active loudspeaker systems with beam steering and controllable directivity. However, most loudspeaker engineers would prefer the presentation in a frequency independent coordinate system following the IEC or other standards as depicted in Figure 1. To express the transfer function  $H(f, \mathbf{r})$  in standard coordinates, each point  $\mathbf{r}_E$  has to be transformed into

$$\mathbf{r} = \mathbf{Q}(f)^{-1}(\mathbf{r}_E(f) + \mathbf{r}_{ref} - \mathbf{r}_{EP}(f)). \quad (33)$$

It is more convenient to export coefficients  $C'_{mn}$  of a modified wave expansion using the standard coordinate system,

$$H(f, \mathbf{r}) = \sum_{n=0}^{N(f)} \sum_{m=-n}^n C'_{mn}(f) \cdot h_n^{(2)}(kr) Y_n^m(\theta, \phi) \quad (34)$$

as illustrated in Figure 1, because the frequency independent orientation and expansion point are identical to the orientation vector  $\mathbf{o}_{ref}$  and the reference point  $\mathbf{r}_{ref}$ . The coefficients  $C'_{mn}(f)$  can be determined by generating virtual data on a sphere with radius  $a$  and performing a similar parameter fitting as described in section 3.4. This expansion is only valid for distances  $r > a$ . For generating a minimum-sized sphere of radius  $a$  that encloses all points of the original scanning grid  $G$ , the required order  $N'(f)$  of the series in standard coordinates is usually significantly higher than the order  $N(f)$  of the series in internal coordinates.

### 5.2. Total sound power

The total sound power radiated by the loudspeaker to infinity can be calculated as

$$\begin{aligned} \Pi(f) &= \frac{1}{2} \int_s \text{Re}\{P(f)V(f)\} dS \\ &= \frac{|U|^2(f)}{2\rho_0 c k^2} \sum_{n=0}^{N'(f)} \sum_{m=-n}^n |C'_{nm}(f)|^2 \\ &= \frac{|U|^2(f)}{2\rho_0 c k^2} \sum_{n=0}^{N(f)} \sum_{m=-n}^n |C_{nm}(f)|^2 \end{aligned} \quad (35)$$

using the orthogonal properties of the spherical harmonics (Parseval theorem). The total sound power can be calculated based on the coefficients  $C'_{mn}$  or  $C_{nm}$  of the internal or standard expansion, respectively.

### 5.3. Apparent power

A useful characteristic for investigating the radial dependency of the sound pressure output is the apparent power

$$\begin{aligned} \Pi_A(f, r) &= \frac{1}{2} \int_s |P(f)| |V(f)| dS \\ &= \sum_{n=0}^{N'(f)} \Pi_{A,n}(f, r) \end{aligned} \quad (36)$$

with the  $n$ th-order wave components

$$\begin{aligned} \Pi_{A,n}(f, r) &= \frac{|U|^2(f) r^2}{2\rho_0 c} \sum_{m=-n}^n |C'_{nm}(f)|^2 \\ &|h_n^{(2)}(kr) \parallel h_{n-1}^{(2)}(kr) - \frac{n+1}{kr} h_n^{(2)}(kr)| \end{aligned} \quad (37)$$

that neglect the phase relationship between particle velocity and sound pressure.

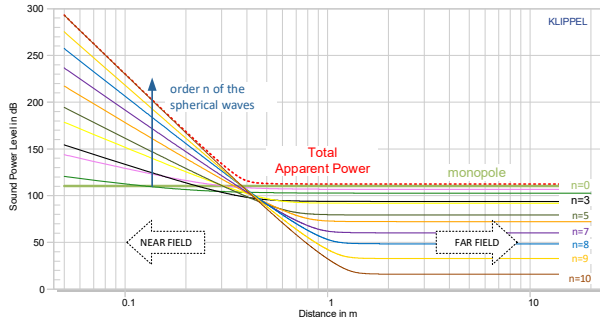


Figure 12 Apparent sound power level (referred to  $10^{-5}$  W for 1  $V_{rms}$  input) of the  $n$ th-order spherical waves and the total expansion at frequency  $f$  as a function of distance  $r$

Figure 12 shows the total apparent power and the contribution of the  $n$ th-order components versus distance  $r$  from the reference point. Only the monopole ( $n=0$ ) generates a constant value because particle velocity and pressure are in phase. The apparent power of the higher-order components ( $n>0$ ) rises in the near field inversely with the distance from the reference point according to Eq. (5). Note that the wave expansion is a very poor approximation of the sound field for distances  $r < a$ .

#### 5.4. Far-Field limit

The general conditions discussed in section 1.1 are only vague criteria for determining the region where the far field conditions are valid. Comparing the difference between apparent and real power level with a useful error limit of 0.5 dB is a convenient way to search for the critical distance  $r_{far}(f)$  as a function of frequency  $f$  in the equation

$$10 \log \left( \frac{\Pi_A(f, r_{far}(f))}{\Pi(f)} \right) dB = 0.5 dB, \quad (38)$$

which considers the particular properties of the device under test.

#### 5.5. Directivity

The directivity factor  $Q$  describes the ratio between the squared sound pressure value at a distance  $r$  on reference axis  $n_{ref}$  and the squared value of an equivalent sound  $p_s(f, r)$  at a distance  $r$  of an omnidirectional virtual source generating the same sound power. This important characteristic can be calculated by

$$Q(f) = \frac{|H(f, r, \theta = 0, \phi = 0)U(f)|^2}{p_s(f, r)^2} = 4\pi \frac{\left| \sum_{n=0}^N \sum_{m=-n}^n C'_{n,m}(f) j^{n+1} Y_n^m(\theta = 0, \phi = 0) \right|^2}{\sum_{n=0}^N \sum_{m=-n}^n |C'_{n,m}(f)|^2} \quad (39)$$

using the coefficients  $C'_{n,m}$  of the standard expansion.

## 6. Visualization

The nearfield holographic measurement provides a lot of valuable information which requires appropriate visual means to simplify the interpretation.

### 6.1. 2D Far Field Data

The amplitude and phase response of the complex transfer function  $H(f, \mathbf{r})$ , depending on a point  $\mathbf{r}$  in the 3D space, can be condensed to 2D information projected on a sphere by considering only the angular dependency at a fixed distance  $r \gg r_{far}$ . This leads to the traditional way of presenting far field as polar, balloon and contour plots as depicted in Figure 13.

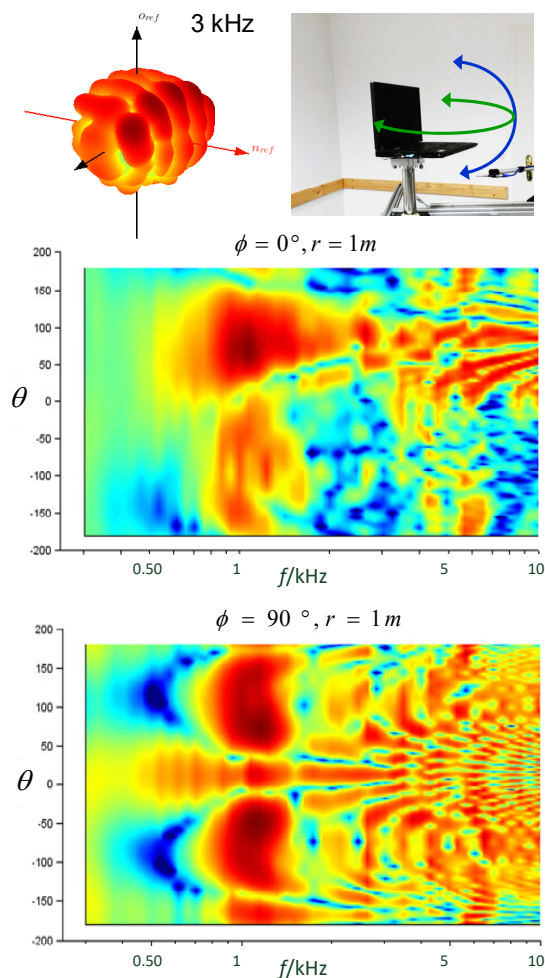


Figure 13 Amplitude of the transfer function  $H(f, \theta, \phi)$  of a laptop measured at a constant distance  $r=1$  m under far field condition, visualized as a balloon plot at  $f=3$  kHz and as a colored contour plot versus latitude angle  $\theta$  for two azimuthal angles  $\phi=0^\circ$  and  $90^\circ$ .

The far field data can be easily extrapolated to any distance  $r(f) > r_{field}(f)$  where the data is accurate. It is also common practice to extrapolate the data to a distance  $r=1\text{m} < r_{field}(f)$  where the near field would generate a deviation if a measurement would be performed at this point. However, this method is very convenient to compare data and to assess the sensitivity of the loudspeaker.

### 6.2. 3D Near field data

The accurate evaluation of the near field data is not only important for personal and portable audio devices such as smart phones, tablets, notebooks, studio monitors, multimedia equipment etc., but also professional loudspeakers where the far field limit  $r_{far}$  is too large for the anechoic room.

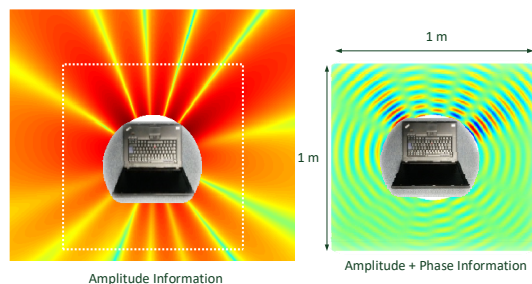


Figure 14 Amplitude and phase of the sound pressure distribution in the near field of a laptop at frequency  $f=3$  kHz.

The amplitude distribution of the transfer function  $H(f, \mathbf{r})$  in the near field of the device can be visualized as an intensity plot over a plane in  $x, y$  coordinates for a selected frequency, as illustrated in the left-hand side of Figure 14. The phase distribution plotted in the same way is more difficult to interpret. It is more intuitive to animate the propagation of a steady state harmonic wave using both amplitude and phase information as illustrated in the right hand side for a selected frequency  $f=3$  kHz. The complete frequency dependency of both amplitude and phase response can be considered by animating the propagating waveform of Dirac impulse over a plane in the near field [10].

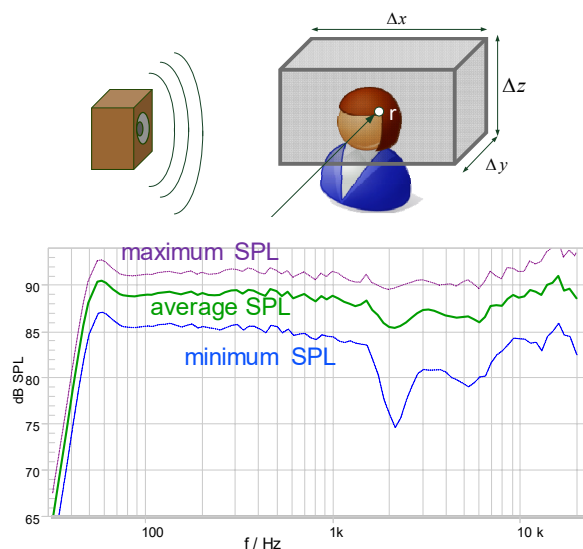


Figure 15 Amplitude and phase of the sound pressure distribution in a personal audio zone.

### 6.3. Audio Zones

Extracting particular features of the sound field on a limited surface or space as illustrated in Figure 15

simplifies the interpretation of the measurement results. For example, the CEA standard 2034 [19] suggests for the evaluation of home consumer loudspeakers the calculation of 5 amplitude responses by averaging the sound pressure distribution on angular sections on a spherical surface in the far field to explain the generation of the direct sound and the interaction with the room. The IEC standard 62777 [20] defines for hand-held and portable audio devices personal audio zones where the statistical properties of the sound field are described by mean, minimum and maximum value as shown in Figure 15.

## 7. Conclusions

The holographic nearfield measurement is an interesting alternative to the traditional far field measurement providing a higher angular resolution and superior accuracy at a significantly reduced measurement time. The nearfield measurement reduces the requirement on the anechoic conditions such as the size of the room, noise suppression and absorption at lower frequency because the direct sound is about 20 dB higher than in the far field. However, the near field measurement cannot be accomplished with conventional turn-tables or microphone arrays but requires a much higher integration of the mechanical scanning process and holographic post processing. An iterative processing exploits early information to adapt the scanning grid and orientation of the internal coordinate system to the particular loudspeaker under test. Thus the new technique overcomes the paradigm that the angular resolution of the measurement grid and directional characteristic is identical. This is key to dynamically minimize the scanning effort necessary for the loudspeaker under test and the particular requirements of the application. The dramatic reduction of measurement points compared to traditional far field measurements allows to scan the sound field with a small redundancy to check the agreement of the wave expansion and the validity of the results. The scanning of the near field of the loudspeaker at multiple layers with different distances to the source is also key for separating the direct sound radiated from the loudspeaker under test from sound waves reflected on the gear and room boundaries, which corrupts the measured sound pressure responses. This sound field separation technique [21] - [24] has the potential to generate more accurate results in normal rooms than by traditional measurements in anechoic rooms.

## 8. REFERENCES

- [1] J. Panzer, D. Ponteggia, "Inverse Distance Weighting for Extrapolating Balloon -Directivity-plots, presented at the 131<sup>st</sup> Convention of the Audio Eng. Soc., 2011 October 20-23, New York, USA, preprint 8473
- [2] R. Aarts, "Comparing Sound Radiation from a Loudspeaker with that from a Flexible Spherical Cap on a Rigid Sphere," *J. Audio Eng. Soc.*, volume 59, issue 4 (April, 2011), pp. 201-212
- [3] E. F. Giron, "Investigations about the Directivity of Sound Sources," Dissertation, Ruhr Universität Bochum, 1996. ISBN 3-8265-1876-4, ISSN 0945-0718 Shaker Verlag GmbH, Aachen.
- [4] J. Vanderkooy, "The Acoustic Center: A New Concept for Loudspeakers at Low Frequencies," presented at the 121<sup>st</sup> Convention of The Audio Eng. Society, 2006 October 5-8, San Francisco, CA, USA.
- [5] Renka, R., "Interpolation of data on the surface of a Sphere and Triangulation and Interpolation of arbitrary Distributed Points in the Plane," *ACM Trans. Math. Softw.* 10, 4 (Dec 1984)
- [6] Shepard, D., "A two-dimensional Interpolation Function of Irregular-Space Data," *ACM Proc. Nat. Conf.* 1968.
- [7] E. Geddes, "Method for Quantifying the Polar Response of Transducers, US 2003/0069710
- [8] D. B. Keele, Jr., "Low-Frequency Loudspeaker Assessment by Nearfield Sound-Pressure Measurement," *J. Audio Eng. Soc.*, vol. 42, pp. 467-482 (1994 June).
- [9] J. Angus, M. Evans "Loudspeaker Pattern Measurement and Representation with Surface Spherical Harmonics," presented at the 104<sup>th</sup> Convention of the Audio Eng. Soc., 1998 May 16-19, Amsterdam, preprint 4717.
- [10] Start, E.W., et al. "Analysis of DDS-Controlled Loudspeaker Arrays by Near Field Acoustic Holography," *Proceedings-Institute of Acoustics*, 2001; 23: 95-110; (15 pages).
- [11] Z. Wang and S. F. Wu, "Helmholtz Equation – Least-Squares Method for Reconstructing the Acoustic Pressure Field," *J. Acoust. Soc. Am.*, vol. 102, pp. 2020-2032 (1997).
- [12] S.F. Wu, "The Helmholtz Equation Least Squares Method for Reconstructing and Predicting Acoustic Radiation, Springer New York, 2015.
- [13] J. Lu, S. Wu, D.B. Keele, Jr., "High-Accuracy Full-Sphere Electro Acoustic Polar Measurements at High Frequencies using the HELS Method," presented at the 121<sup>st</sup> Convention of the Audio Eng. Soc., San Francisco, CA, USA, 2006 October 5-8, preprint 6881.
- [14] F. Zotter, "Analysis and Synthesis of Sound - Radiation with Spherical Arrays," Dissertation University of Music and Performing Arts, Austria, September 2009
- [15] B. Rafealy, "Analysis and Design of Spherical Microphone Arrays," *IEEE Trans. on Speech and Audio Processing*, 2005, 13(1): 135-143.
- [16] B. Rafealy, et. al. "Spatial Aliasing in spherical Microphone Arrays," *IEEE Trans on Signal Proc.*, 2007, 55(3):1003-1010.

- [17] C. Deeg, "Holgrafische Bestimmung der Abstrahlcharakteristik von Lautsprechern im Voll- und Halbraum" Diplomarbeit TU Dresden, Fakultät Elektrotechnik, 2013.
- [18] F. Fazi, et. al. "Measurement and Fourier-Bessel Analysis of Loudspeaker Radiation Patterns using a spherical array of Microphones," presented at the 124<sup>th</sup> Convention of the Audio Eng. Society, 2008.
- [19] CEA-2034, Standard Method of Measurement for In-Home Loudspeakers, ANSI/CEA Standard, November 2013.
- [20] IEC 62777, "Quality evaluation method for the sound field of directional loudspeaker array system, Standard of the International Electrotechnical Commission, 2016
- [21] G. Weinreich and E. B. Arnold, "Method for Measuring Acoustic Radiation Fields," J. Acoust. Soc. Am. 68(5), 404-411 (1980).
- [22] M. Melon, et. al. "Comparison of four subwoofer Measurement Techniques," J. Audio Eng. Soc. 55(12), pp. 1077-1091 (2007).
- [23] Q. Zhu, M. Wu, J. Yang, "Methods for Measuring Spatial Radiation Patterns of Loudspeakers," Int. Symposium on ElectroAcoustic Techn, Shenzhen, 2015, China.
- [24] M. Melon, et. al. "Evaluation of a method for the measurement of subwoofers in usual rooms. J. Acoust. Soc. Am., 2010, 127(1), 256-263.